Journal of Electroanalytical Chemistry 823 (2018) 106–120

Contents lists available at ScienceDirect

Journal of Electroanalytical Chemistry

journal homepage: www.elsevier.com/locate/jelechem

Electrodeposition of indium on W and Cu electrodes in the deep eutectic solvent choline chloride-ethylene glycol (1:2)

E. Barrado[a,*], S. García[a], J.A. Rodríguez[b], Y. Castrillejo[a]

[a] UIC090, Dpto de Química Analítica, Facultad de Ciencias, Universidad de Valladolid, Paseo de Belén 7, 47011 Valladolid, Spain
[b] Centro de Investigaciones Químicas, Universidad Autónoma del Estado de Hidalgo, Carr. Pachuca-Tulancingo Km. 4.5, 42076 Pachuca, Hidalgo, Mexico

ARTICLE INFO

Keywords:
Deep eutectic solvents
Indium
Disproportionation
Diffusion coefficient
Cu-in intermetallic compounds

ABSTRACT

A procedure for drying the deep eutectic solvent (DES) choline chloride - ethylene glycol, ChCl-EG (1:2), based on the use of molecular sieves has been developed, being the final water content of the electrolyte 145 ± 5 ppm. In this dried DES, the stability of InCl and $InCl_3$ as well as the electrochemical behaviour of their solutions has been investigated using electrochemical techniques, X-ray diffraction analysis (XRD) and scanning electron microscopy (SEM). Experiments performed under a N_2 atmosphere show that $InCl_3$, dissolved in the rich chloride media as $InCl_p^{3-p}$, is reduced on a tungsten electrode to indium metal via only one electrochemical step. Conversely, InCl undergoes the following disproportionation reaction when dissolved in the eutectic ChCl-EG (1:2)

$$3InCl(s) + (p-3)Cl^- \rightleftharpoons 2In(0) + InCl_p^{3-p}$$

generating In(0) and giving place to identical electrochemical signals as those obtained after the addition of $InCl_3$ to the DES.

On a tungsten electrode, nucleation and crystal growth of In plays an important role in the electrodeposition process. Chronoamperometric results were consistent with instantaneous three dimensional nucleation on a finite number of active sites with diffusion controlled growth of the nuclei, whatever the applied overpotential and temperature. Mass transport towards the electrode is a diffusion process, and the following empirical expression for the temperature dependence of the diffusion coefficient was calculated.

$$LnD = -(3.58 \pm 0.22) - (3665 \pm 76)\,T^{-1}$$

The electro-reduction of In(III) solutions was also investigated at a copper substrate. The resulting cyclic voltammograms evidenced the formation of In-Cu intermetallic compounds. Hence, In-Cu alloy films were obtained by continuous potentiostatic electrolysis and intensiostatic pulse electrolysis. The obtained samples, characterized by XRD and SEM, revealed the formation of the metastable CuIn phase that could be transformed into $Cu_{11}In_9$ by thermal annealing.

1. Introduction

Indium and its alloys are suitable materials for producing semiconductor compounds such as the binaries (InP, InSb, InAs), ternaries (InGaP, GaInAs, $CuInSe_2$,) and quaternaries (CuInSSe and $Cu(In,Ga)Se_2$) which are widely used in electronic and optoelectronic technology [1–3]. In this context, polycrystalline thin films of the chalcopyrite materials $CuInSe_2$ and $Cu(In,Ga)Se_2$ are proposed as absorbent materials for photovoltaic solar cells, due to their high optical absorption coefficient of approximately 10^{-5}, and p-i-n-type electrical conductivity with band gaps of 1.0 eV for $CuInSe_2$ and 1.09 eV for $Cu(In,Ga)Se_2$ respectively, [2, 3].

Electrosynthesis is an attractive option to prepare advanced materials under the form of coatings or thin layers, due to its many advantages: i) economics (e.g. low investment is required for an easy composition control, with large coverage areas and high deposition rates), and ii) ecologic (no product loss, and efficient use of raw materials) [3, 4]. The processes to prepare chalcopyrite absorber layers involve electrodeposition of precursor films of Cu-In alloy, $CuInSe_2$, $Cu(In,Ga)Se_2$ followed by re-crystallization by thermal annealing at high

* Corresponding author.
E-mail address: ebarrado@qa.uva.es (E. Barrado).

https://doi.org/10.1016/j.jelechem.2018.06.004
Received 9 April 2018; Received in revised form 30 May 2018; Accepted 2 June 2018
Available online 04 June 2018
1572-6657/

temperature in selenium atmosphere [2]. The most usual approach to electrodeposit metal and alloys takes place in aqueous solutions. Nevertheless, aqueous electrolysis presents an important shortcoming; the hydrogen discharge that hinders the electrodeposition of very electronegative elements such as Ga and In, reduces the plating efficiency, and has destructive impacts on the thin film quality causing the appearance of pinholes and dendritic morphologies [5].

An alternative to aqueous electroplating solutions is to use as electrolytes low cost room temperature ionic liquids, as the deep eutectic solvents (DES) based on combinations of choline chloride with urea or ethylene glycol. DES exhibit important properties, including high conductivity, relatively wide potential range of electrochemical stability, low vapor pressure, and ability to solvate many metal salts [6]. All these properties make DES good candidates to be used as electrolytes for the electrodeposition of metals [7, 8], alloys [9] and semiconductors [2, 5].

Electrodeposition of precursor films of Cu-In alloy, $CuInSe_2$, Cu(In,Ga)Se_2 deals with the electrochemical behaviour of several elements, each of them with specific electrochemical properties, making the overall system very complex. Therefore, the electrochemical production of precursor films can only be rationally conceived via a deep understanding of the chemistry and electrochemistry of the elements in the selected electrolytic bath. In this context, the present work examined the feasibility of using the mixture choline chloride (ChCl)-ethylene glycol (EG) in the eutectic composition, ChCl-EG (1:2), for the electrodeposition of In on different substrates: i) W, as an inert material, and ii) Cu, a metal with possibility of alloy formation. The electrochemical behaviour of $InCl_3$ and InCl solutions on the W substrate have been studied, to our knowledge for the first time, by using electrochemical techniques, including cyclic voltammetry, chronoamperometry and chronopotentiometry. The electrodeposition of Cu-In alloys is also reported, being the obtained electrodeposits analysed by X-ray diffraction analysis (XRD), scanning electron microscopy (SEM) and energy dispersive X-ray spectroscopy (EDX).

2. Experimental

2.1. Molecular sieve "activation" (drying)

Before using molecular sieves as a drying agent, they must be "activated" by removing all traces of water and other volatile compounds. Therefore, the appropriate amount of molecular sieve 4A was added to a dry flask and heated in a microwave for 2 min at 500 W (no stirring needed). The flask was immediately connected to a vacuum pump. When the flask had cooled down to room temperature (in approximately 15 min), the flask was isolated from the vacuum pump, and purged with dry dinitrogen (Alphagaz N_2 (1) purchased from Air Liquide) for 3 min. By repeating the process again three times, the molecular sieves are "activated" (dried) and ready to use.

2.2. Solvent preparation

The electrolytic medium was prepared by mixing analytical grade of choline chloride ($HOC_2H_4N(CH_3)_3Cl$, Sigma-Aldrich > 98%) and ethylene glycol ($HOCH_2CH_2OH$, Sigma-Aldrich 99.8%) in a 1:2 M ratio (ChCl-EG (1:2)). This mixture was kept in an oven at 70 °C until a colourless homogeneous liquid was formed. Due to the hygroscopicity of the solvent, activated molecular sieve was added to the mixture in a proportion of 15 g per 100 mL of ChCl-EG (1:2). Afterwards, the container was hermetically closed with a Septum and an atmosphere of N_2 was maintained by means of a balloon. The dried solvent can be used after 10 days (i.e. when the water content remains constant).

Karl-Fischer analysis was performed to determine the water content of the electrolyte, using an automatic titrator (Mettler Toledo C20 KF Coulometer). The water content of the dried DES was 145 ± 5 ppm.

The density and viscosity of the solvent, gathered in Table 1, were also determined at several temperatures by using a Stabinger Viscometer SVM 3000, Anton Paar. The experimentally measured density of ChCl-EG (1:2) is found to vary lineally with the absolute temperature and was fitted to the following equation:

$$\rho(\mathrm{g\ cm^{-3}}) = (1.2835 \pm 0.0008) - (5.529 \pm 0.024) \times 10^{-4} \times T \quad (1)$$

Although the measured viscosity of ChCl-EG (1:2) may be described by the simplest Arrhenius model over the temperature range studied (293–373 K), the Vogel − Fulcher − Tamman (VFT) model appears to more satisfactorily describe the viscosity as follows:

$$\eta(mPa.\ s) = (0.07614)\ exp\ \frac{1046.22}{[T - 137]} \quad (2)$$

2.3. The cell

A portion of the electrolyte, stored in an airtight glass bottle, was transferred to the electrochemical conical cell with thermostat jacket, Metrohm 6.1418.150, made of glass to enable visual inspection of the electrodes and electrolyte. The cell was connected to a TAMPSON TC6B thermostat in order to control the temperature to ± 1 K, and dry dinitrogen (Alphagaz N_2 (1)) was bubbled through the solution continuously to ensure the absence of oxygen and water.

Later, the required mass of anhydrous $InCl_3$ (Sigma Aldrich > 99.999%), and InCl (Sigma Aldrich 99.999%), stored in a MBaun Labstar 50 glove box in Ar atmosphere, were added to the dried solvent.

2.4. Electrochemical measurements

The reference electrode, consisted of a silver wire (Sigma Aldrich 99.9% φ = 1 mm) dipped into an electrolyte vessel (Metrohm 6.1240.000) with PTFE capillary and ceramic diaphragm (3 mm), filled with a solution 0.10 mol kg^{-1} AgCl in the mixture ChCl-EG (1:2). Unless otherwise stated, all potentials are referred to this reference Ag (I)/Ag.

For cyclic voltammetry, and pulse techniques, a tungsten, W, rod (Metrohm 6.1248.050 φ = 2 mm), a glassy carbon, GC, rod (Metrohm 6.1248.040 φ = 2 mm), and a copper, Cu, wire (Sigma Aldrich φ = 1 mm) were used as working electrodes. As counter electrode a GC rod (Sofacel φ = 3 mm) was used.

Potentiostatic and intensiostatic electrolysis were conducted with both a 0.25 mm thick tungsten foil (Sigma Aldrich, 99.999%) and a 0.5 mm thick copper foil (Sigma Aldrich 99,98%), as cathodes and a glassy carbon rod (Sofacel) as counter electrode.

The electrochemical experiments were carried out under a N_2 atmosphere with: (i) a PAR EG&G Model 273A potentiostat/galvanostat controlled by a computer using the EG&G M270 software package and (ii) an Autolab PGSTAT 320N potentiostat/galvanostat controlled by the research software NOVA 1.10.

2.5. Deposit characterization

After electrolysis, samples were cleaned by immersion in ultrapure water Milli-Q, and finally in ethanol. X-ray diffraction (XRD) measurements were performed using a Bruker D8 Discover A25 X-Ray diffractometer with CuKα radiation (40 kV, 30 mA). The surface morphology was analysed with a scanning electron microscope (SEM, FEI Model Quanta 200F) equipped with energy dispersive spectroscopy (EDAX, SDD Apolo) for characterization of the elemental composition.

Table 1
Variation of the diffusion coefficient of In(III) with the temperature in the DES ChCl-EG (1:2) calculated by different electrochemical techniques, density (ρ), dynamic viscosity (η), kinematic viscosity (ν), and Schmidt number.

D $InCl_p^{3-p}/10^{-7}\ cm^2\ s^{-1}$						
T/K	313	323	333	343	353	363
CA		3.99 ± 0.15		7.64 ± 0.26		12.88 ± 0.33
CP		2.99 ± 0.17		6.01 ± 0.20		9.61 ± 0.34
CPSV	2.47 ± 0.06	3.22 ± 0.83	4.79 ± 0.11	6.70 ± 0.09	9.52 ± 0.22	12.17 ± 0.39
Mean value	2.47 ± 0.06	3.25 ± 0.35	4.79 ± 0.11	6.56 ± 0.59	9.52 ± 0.22	11.43 ± 1.43
$\rho/kg\ m^{-3}$	1110.4	1104.7	1099.2	1093.6	1088.1	1082.7
$\eta/kg\ m^{-1}\ s^{-1}$	0.028940	0.020967	0.015848	0.012238	0.0096892	0.0077822
$\nu/cm^2\ s^{-1}$	0.26063	0.18980	0.14418	0.11191	0.089047	0.071878
$Sc/10^4$	105.5	58.4	30.1	17.1	9.4	6.3

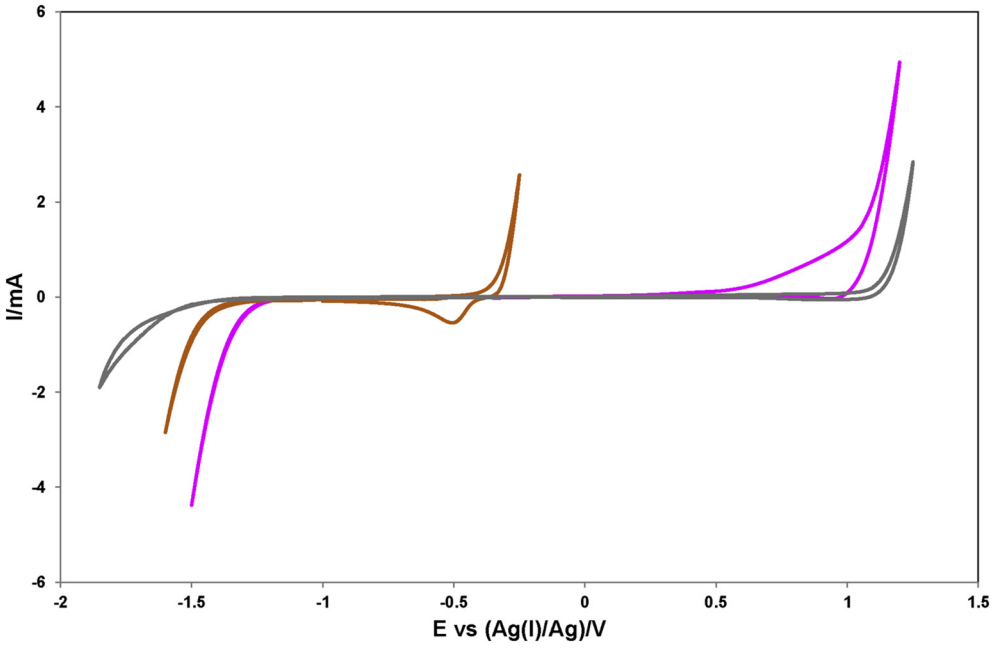

Fig. 1. Electrochemical window on GC (—), W (—) and Cu (—) electrodes in the deep eutectic solvent ChCl-EG (1:2) at 343 K.

3. Results and discussion

3.1. Electrochemical window of the ChCl-EG (1:2) on GC, W and Cu electrodes

Fig. 1 depicts examples of the electrochemical window achieved in the eutectic ChCl-EG (1:2) mixture at 343 K when the aforementioned working electrodes were used.

On GC and W substrates, the anodic limit of the electrochemical window is due to the oxidation of the chloride ions of the solvent into chlorine by means of the reaction:

$$2Cl^- - 2e^- \rightarrow Cl_2(g) \quad (3)$$

On the contrary to the results reported by Haerens et al. [10], the chlorine emission has been identified, to our knowledge for the first time, in macro-electrolysis experiments using as anode and cathode W plates and GC rods in their 4 possible combinations, being N_2 continuously bubbled in the proximity of the anode. With the aim to collect the released $Cl_2(g)$ and generate hypochlorite ions (Reaction (4)), the gasses were passed over a NaOH solution 0.25 mol L^{-1}, and the obtained solution was treated with KI and H_2SO_4 to generate I_3^- (Reaction (5)), that was extracted with Cl_4C giving a pink colour to the organic phase (Fig. 2.a).

$$Cl_2 + 2OH^- \rightleftharpoons Cl^- + OCl^- + H_2O \quad (4)$$

$$2OCl^- + 3I^- + 2H_3O^+ \rightleftharpoons 2Cl^- + I_3^- + 3H_2O \quad (5)$$

The chlorine emission was also detected placing in the proximity of the anode a filter paper strip impregnated with a solution of KBr and fluorescein ($C_{20}H_{12}O_5$). In the presence of Cl_2, pink eosin ($C_{20}H_8Br_4O_5$) is generated (Fig. 2.b) according to the following reactions [11]:

$$Cl_2(g) + 2Br^- \rightleftharpoons 2Cl^- + Br_2(g) \quad (6)$$

$$4Br_2 + C_{20}H_{12}O_5 + 4H_2O \rightleftharpoons 4\,Br^- + C_{20}H_8Br_4O_5 + 4H_3O^+ \quad (7)$$

On the other hand, if the solubility of chlorine in the solvent is high enough, some of the $Cl_2(g)$ formed at the anode could react with the Cl^- ions of the solvent giving Cl_3^-.

$$Cl_2(g) + Cl^- \rightarrow Cl_3^- \quad (8)$$

The presence of Cl_3^- in the solution used in the macro-electrolysis experiments was also tested by UV–Vis using a *Hewlett Packard 8453 (G1103A) Diode-Array Spectrophotometer*. As can be seen in Fig. 3, the spectrum shows a maximum absorbance at approximately 220 nm, which corresponds relatively well with the value reported by Haerens et al. [10] for Cl_3^- in the same solvent.

Conversely, at a Cu electrode the anodic region is limited by the dissolution of the electrode material, according to the following reaction:

$$Cu(0) - 1e^- \rightarrow Cu(I) \quad (9)$$

On the three working electrodes, the cathodic limit of the electrochemical window occurs simultaneously with the formation of small bubbles on the electrode surface, and can be assigned to the reduction

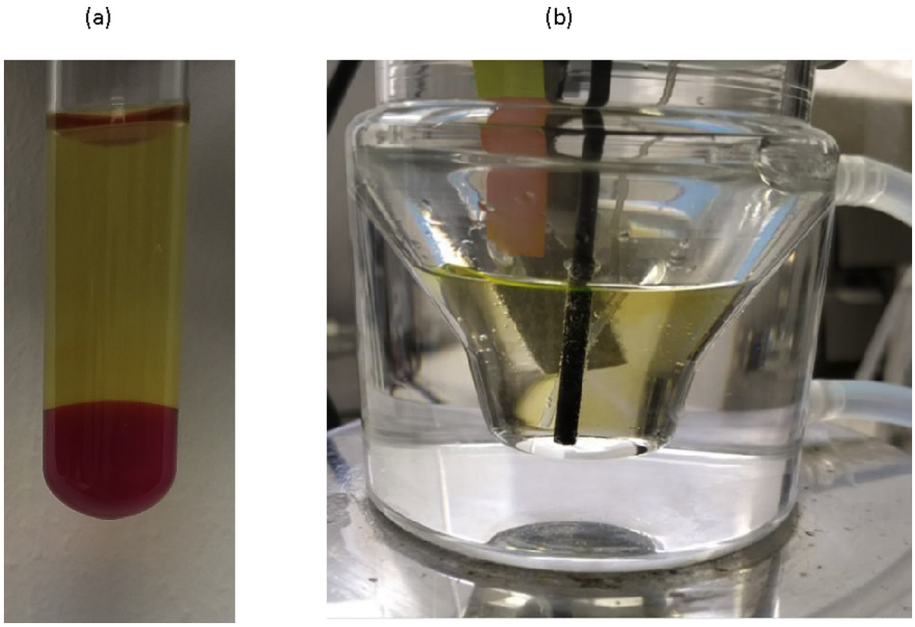

Fig. 2. Chlorine detection: (a) photo of the aqueous and organic phase after extraction of I_3^- (b) filter paper strip impregnated with fluorescein ($C_{20}H_{12}O_5$) and KBr, showing the formation of pink eosin ($C_{20}H_8Br_4O_5$). (For interpretation of the references to colour in this figure legend, the reader is referred to the web version of this article.)

of the hydroxyl groups of ethylene glycol (EG), choline ions (Ch^+) or traces of water with formation of H_2 (g) [7, 12, 13]. As can be seen in Fig. 1, hydrogen evolution depends on the electrode material, a phenomenon previously reported by Vieira et al. [13].

3.2. Stable oxidation states of indium in the eutectic ChCl-EG (1:2)

a) Results obtained with addition of $InCl_3$

$InCl_3$ dissolved in the rich chloride solvent producing a colourless solution with the formation of $InCl_p^{3-p}$ complex [1, 14] hereafter In(III). An example of the cyclic voltammograms obtained with a solution of In (III) 7.29×10^{-5} mol cm^{-3} on a tungsten electrode at 343 K is displayed in Fig. 4. The electroreduction of In(III) proceeds via a one step process, being developed a peak marked as "I_c" with the wonted shape for the formation of a new phase, steep rise of the cathodic current and slow decay. In the reverse scan, a peak "I_a" is built up, which corresponds to the reoxidation of the indium metal deposited during the cathodic scan. On top of that, an important nucleation loop can be observed in the voltammograms, indicating that the onset of massive deposition of In requires the application of an important overpotential [15].

In order to prove the formation of metallic indium, intensiostatic pulse electrolysis was conducted on W foils from the electrolyte containing In(III). Each pulse consists of an ON-Time (t_{ON}) during which a current is applied, and an OFF-Time (t_{OFF}) during which no current is applied. The solution was stirred by bubbling dried N_2 during the experiments. After the electrolysis, the deposits were washed with ultrapure water and ethanol and analysed by XRD (Fig. 5) and SEM-EDAX (Fig. 6 (a–b)). In all the cases the deposits consist of pure metallic indium. Moreover, the deposits present a homogeneous morphology (Fig. 6a) with small clusters of particles with the tetragonal crystal

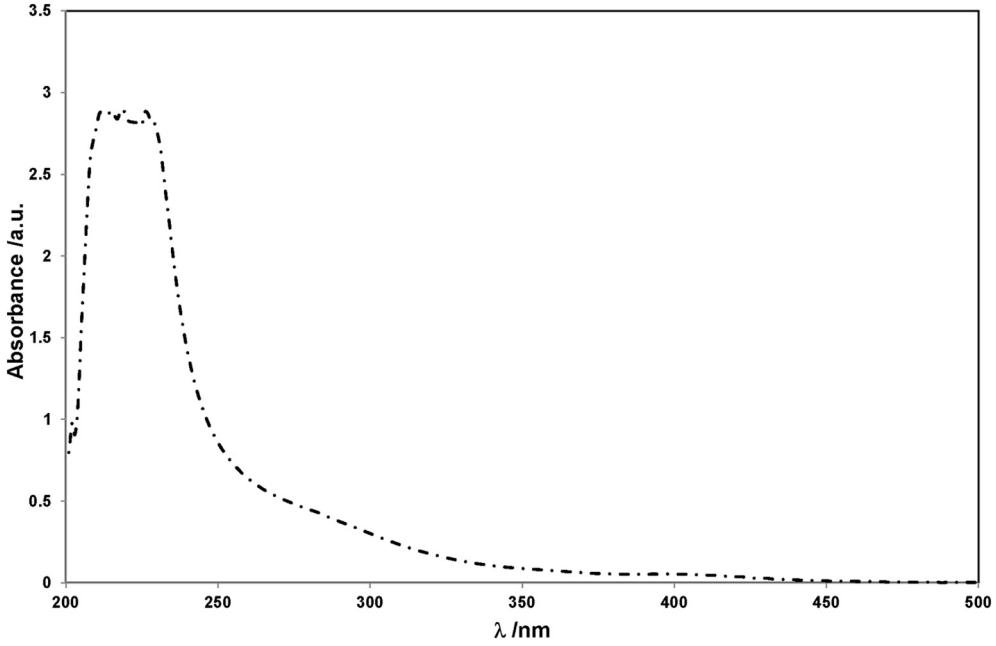

Fig. 3. UV–Vis spectrum of the eutectic ChCl-EG (1:2) after electrolysis using as reference pure ChCl-EG (1:2).

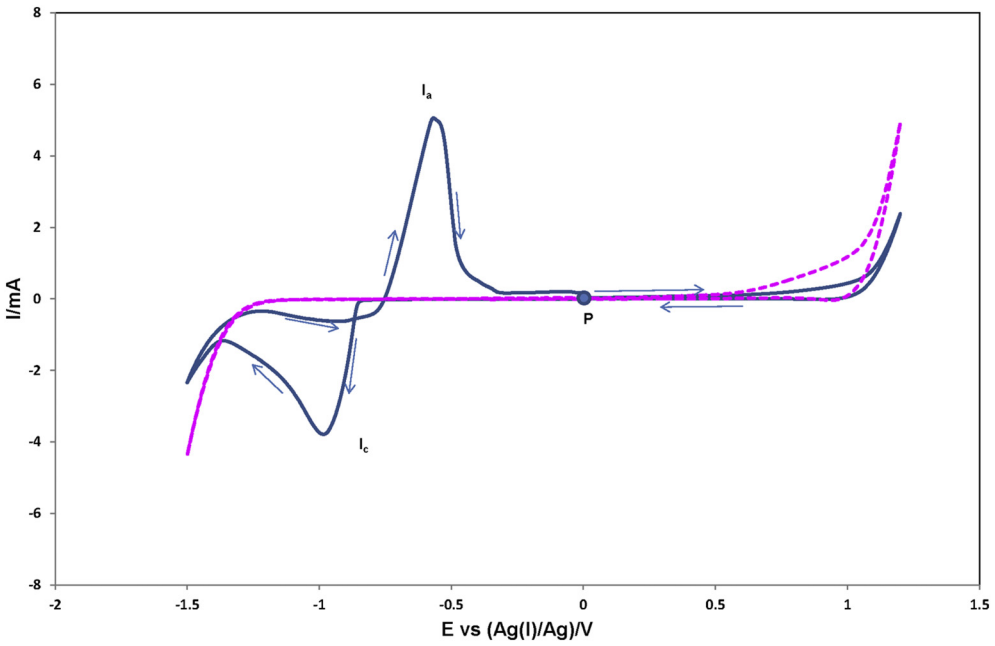

Fig. 4. Cyclic voltammogram obtained with a solution of $InCl_p^{3-p}$ ($C_0 = 7.29 \times 10^{-5}$ mol cm^{-3}) on a tungsten electrode at 100 mV s^{-1} and 343 K. Pink line corresponds to a cyclic voltammogram of the ChCl-EG (1:2) in absence of $InCl_p^{3-p}$. (For interpretation of the references to colour in this figure legend, the reader is referred to the web version of this article.)

structure (Fig. 6b).

Taken together, the foregoing results lead to the conclusion that the electrochemical signal I_c displayed in Fig. 4 was due to the following reaction:

$$InCl_p^{3-p} + 3e^- \rightarrow In(0) + p\ Cl^- \quad (10)$$

b) Results obtained with addition of InCl(s)

The addition of anhydrous InCl(s) to the solvent gives place to a colourless solution and a solid with metallic appearance at the bottom of the cell. *Al* first glance, the voltammograms obtained with this solution and illustrated in Fig. 7, appeared to be identical to those shown in Fig. 4, indicating the presence of $InCl_p^{3-p}$ in solution, and suggesting that InCl has undergone the following disproportionation reaction when dissolved in the DES:

$$3InCl + (p-3)\ Cl^- \rightleftharpoons 2In + InCl_p^{3-p} \quad (11)$$

In order to endorse the disproportionation of InCl, the solid formed at the bottom of the cell was analysed by XRD (Fig. 8) and SEM-EDAX (Fig. 9) being confirmed the presence of metallic indium.

3.3. Electrochemical nucleation of indium on a tungsten electrode in the eutectic ChCl-EG (1:2)

The nucleation/growth process of indium on a tungsten electrode

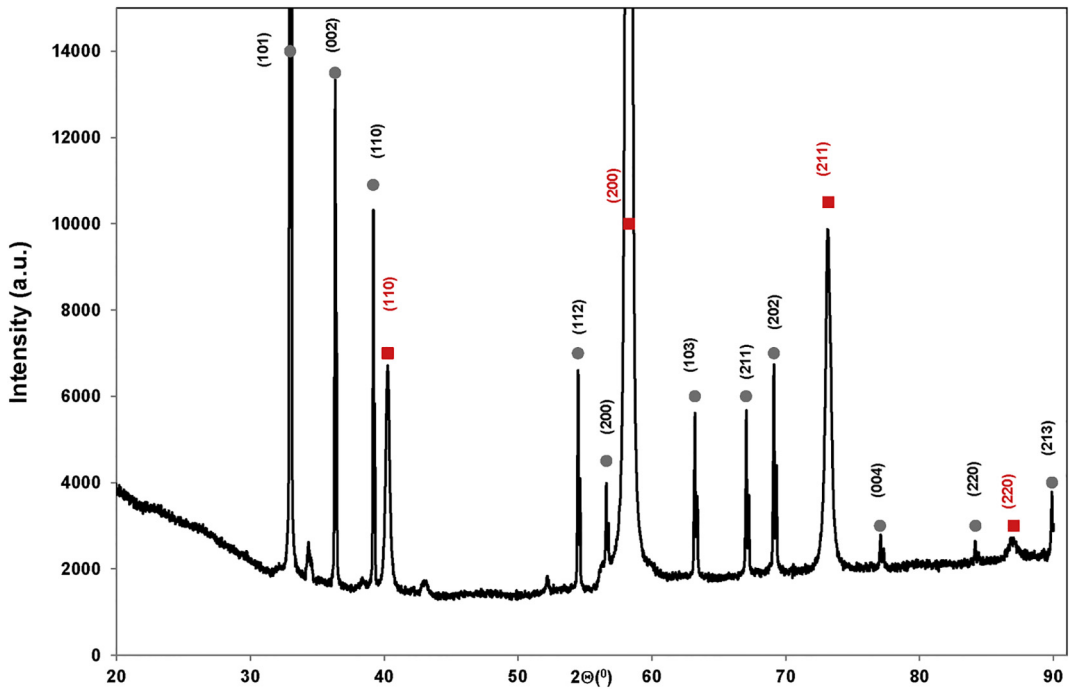

Fig. 5. XRD pattern of In films obtained on a W foil from the electrolyte containing $InCl_p^{3-p}$ under galvanostatic intermittent electrolysis ($J_{app} = -6.5$ mA cm^{-2}, $t_{off} = 2$ s $t_{on} = 5$ s, $t_{total\ elec} = 72$ min). (●) In, (■) W.

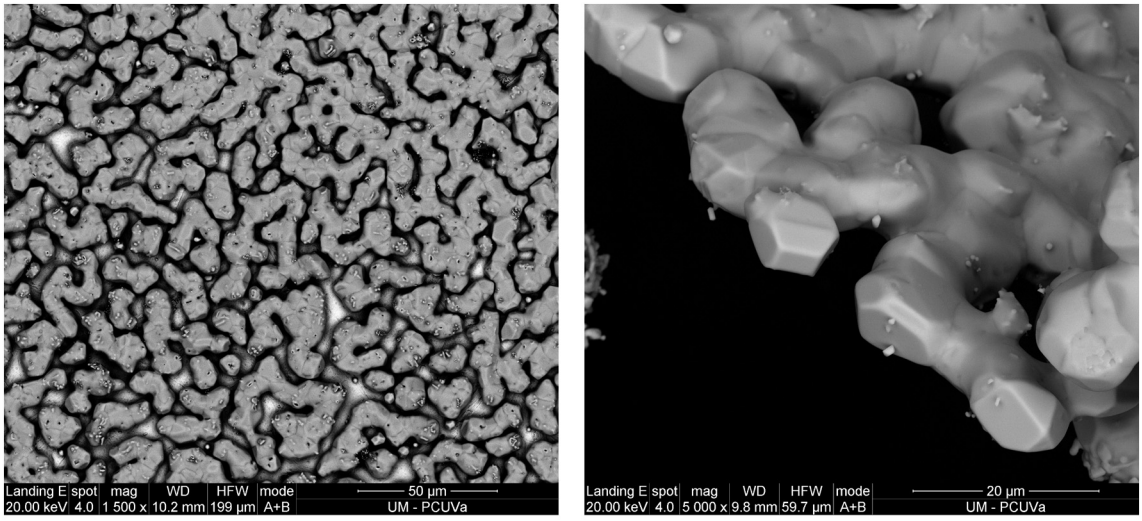

Fig. 6. SEM micrographs of a W foil coated by an In film (a) surface appearance, (b) details.

was studied with a solution of In(III), analyzing the chronoamperometric responses to single potential steps. With the aim to obtain accurate results the electrode and the diffusion layer must be renewed before each measurement. Therefore, the following renewal procedure of the electrode/electrolyte interface was applied:

1) after every potential-step measurement, the solution was stirred and the electrode polarized for 120 s at a potential value sufficiently anodic to ensure that the deposited indium metal was totally removed from the surface
2) afterwards, the solution stirring was stopped and 15 s were waited without applying any voltage before running the new measurement.

Fig. 10 shows examples of the responses resulting from such experiments. In the very beginning, each transient displays a current spike due to the charging of the electrode double layer, which is followed almost immediately by a rising current due to the formation and growth of indium nuclei. The rising part of the current culminates in a current maximum, i_m, at a time t_m. The values of i_m and t_m depend on the magnitude of the potential step (i.e. i_m achieves greater values and t_m decreases when the applied potential is more cathodic). Finally the current decays converging at long times to the limiting behaviour described by the Cottrell equation.

With the aim to identify the indium nucleation mode, the dimensionless experimental current-time transient obtained at several cathodic potentials and temperatures were compared to the theoretical model derived by Scharifker and Hills [16]. The model distinguishes between the two limiting nucleation mechanism: i) instantaneous nucleation that corresponds to a rapid nucleation on a fixed number of active sites and ii) progressive nucleation at a more slowly rate on an infinite number of active sites [17]. Scharifker and Hills model includes algebraic expressions for instantaneous and progressive nucleation as shown in Eqs. (12) and (13) respectively [16].

$$\left(\frac{I}{I_m}\right)^2 = 1.9542\frac{[1-\exp(-1.2564(t/t_m))]^2}{(t/t_m)} \quad (12)$$

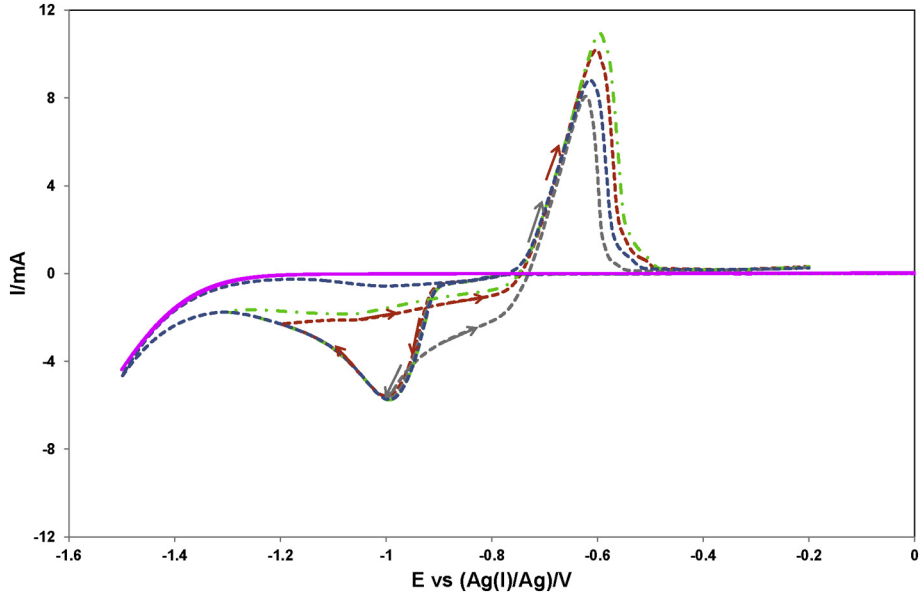

Fig. 7. Cyclic voltammograms recorded at different inversion potentials on a tungsten electrode at 100 mV s^{-1} and 343 K after the addition of anhydrous InCl to ChCl-EG (1:2).

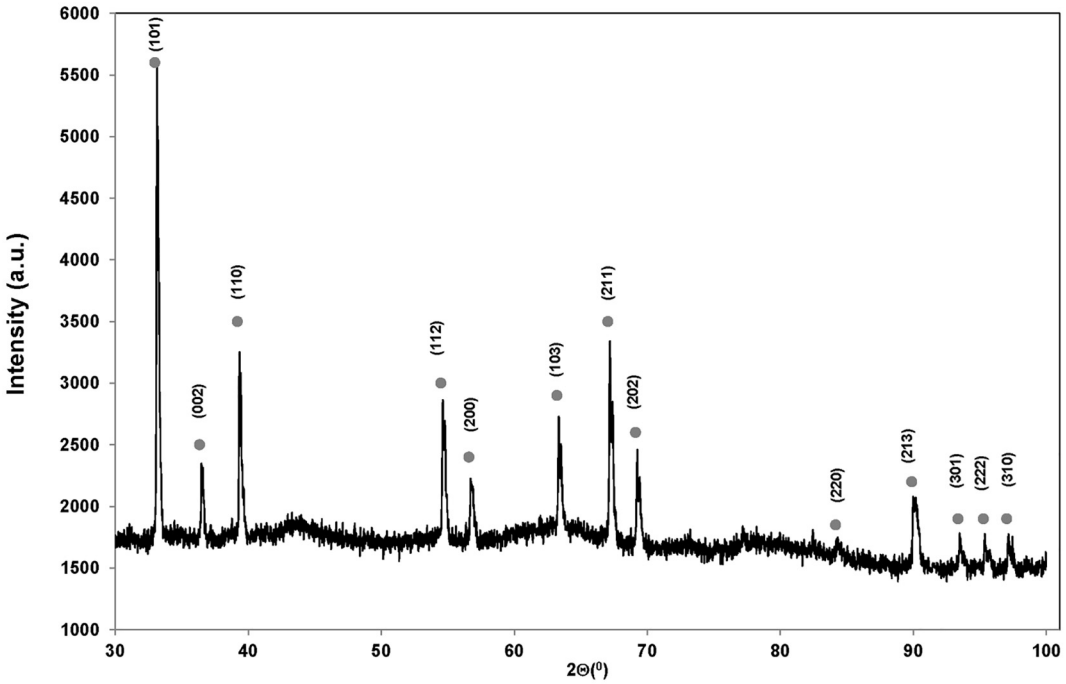

Fig. 8. XRD pattern of the solid formed at the bottom of the cell after the addition of anhydrous InCl(s) to the DES (●) In.

$$\left(\frac{I}{I_m}\right)^2 = 1.2254\frac{[1-\exp(-2.3367(t/t_m)^2)]^2}{(t/t_m)} \quad (13)$$

In order to make a better comparison between the nucleation model and experimental results, the induction time, t_0, between the application of the potential step and the onset of nucleation and growth has to be taken into account [18–21]. Estimates of t_0 can be obtained from the intercept of the plots of $(i/i_m)^2$ vs t and$(i/i_m)^{2/3}$ vs t for instantaneous and progressive nucleation respectively [20, 21].

Plots of $(i/i_m)^2$ vs (t'/t'_m) (being $t' = t - t_0$, $t'_m = t_m - t_0$) calculated from Eqs. (12) and (13) are shown in Fig. 11 together with the dimensionless experimental data, taken from the chronoamperometric curves as those gathered in Fig. 10. According to Fig. 11 the initial stages of electrochemical deposition of indium onto a tungsten electrode in the deep eutectic solvent ChCl-EG (1:2) can be explained in terms of a model involving instantaneous nucleation with three-

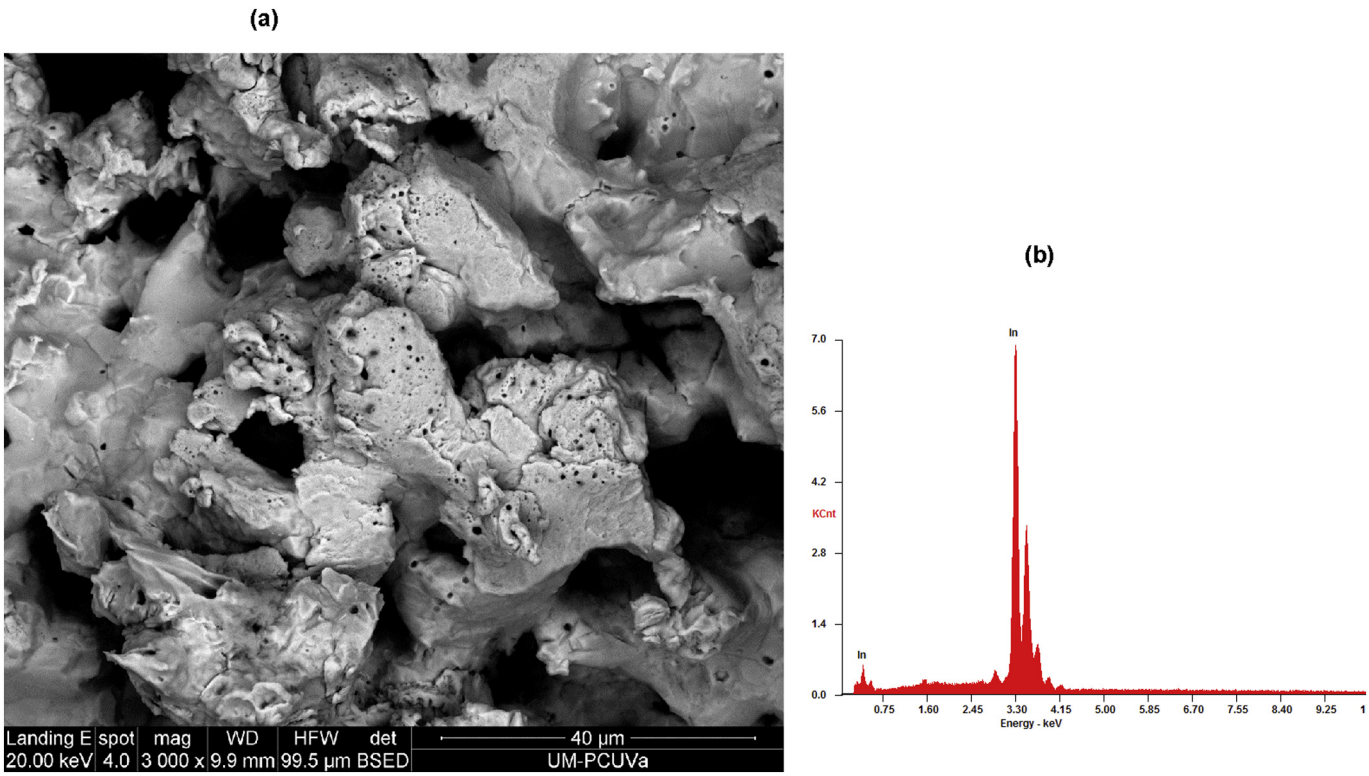

Fig. 9. (a) SEM micrograph of the solid formed at the bottom of the cell after the addition of anhydrous InCl(s) to the DES. (b) EDX analysis.

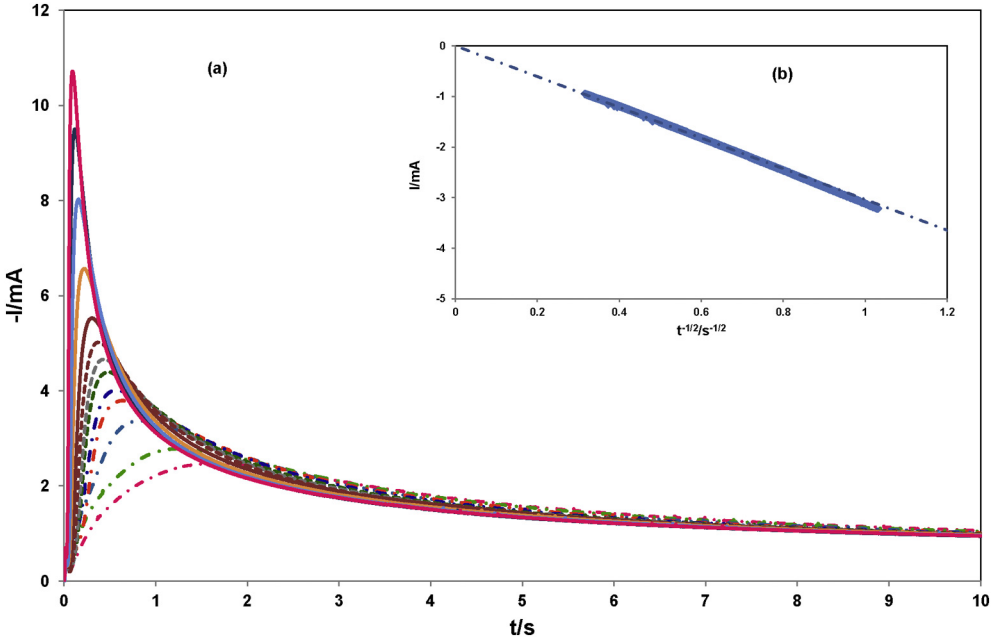

Fig. 10. (a) Evolution of the chronoamperograms of a $InCl_p^{3-p}$ solution ($C_0 = 6.21 \times 10^{-5}$ mol cm^{-3}) at a tungsten electrode ($S = 0.46$ cm^2) at various applied potentials −0.870 (–); −0.890(–); −0.920 (–); −0.930 (–); −0.940 (–); −0.950 (–); −0.970 (–); −1.000 (–); −1.020 (–); −1.040 (–); −1.060 (–); 1.080 (–) and −1.100 (–) V vs Ag(I)/Ag, at 323 K. (b) Relation between square root of time and current at potential values (e.g. E = −1.100 V) where the reaction is diffusion controlled.

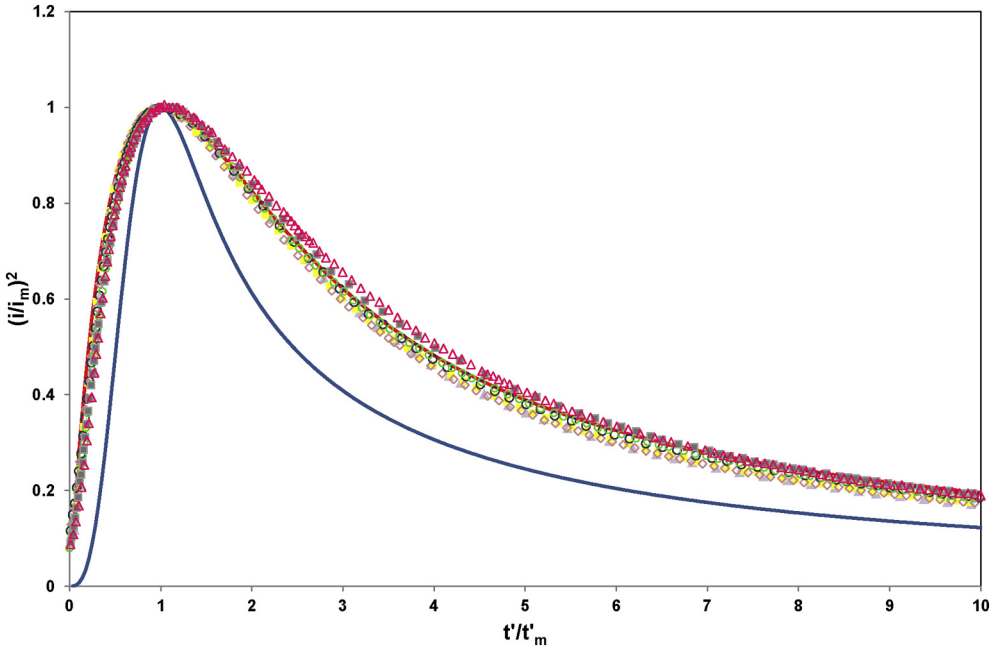

Fig. 11. Comparison of the dimensionless experimental data obtained from the current-time transients, represented in Fig. 10, with the theoretical model for (–) instantaneous and (–) progressive nucleation at various applied potentials. (Δ) −0.930, (■) −0.970, (●) −1.000, (◇) −1.040, (■) −1.060, (○) −1.020, (▲) −1.080 V vs (Ag (I)/Ag.

dimensional growth of the nuclei whatever the applied overpotential. On the other hand, the nucleation mode of indium is not influenced by temperature in the 323–363 K range.

3.4. Determination of the $InCl_p^{3-p}$ diffusion coefficient. Verification of the Arrhenius's law

Chronoamperometry (CA), chronopotentiometry (CP) and convolutive potential sweep voltammetry (CPSV) seem to be relevant techniques for the determination of the diffusion coefficient of $InCl_p^{3-p}$, $D_{In(III)}$, in the deep eutectic solvent ChCl-EG (1:2), on condition that the adequate equations in the appropriate experimental conditions are used. The aim of the work is to identify if the three methods yield identical results or one among them is more appropriate than the others considering: i) the accuracy of the measurements, and ii) the simplicity of data acquisition [22].

3.4.1. Results obtained by chronoamperometry (CA)

The diffusion coefficient of In(III) was calculated from the chronoamperometric responses obtained with a solution of In(III) at potential values in the mass-transport controlled region (i.e. where the surface concentration of In(III) is effectively zero). Fig. 10 (b) shows the variation of the current versus $1/t^{1/2}$, confirming that the experimental data obey the Cottrell law [15, 23, 24].

$$I_d(t) = \frac{nFSD^{1/2}C_0}{\pi^{1/2}t^{1/2}} \tag{14}$$

where $I_d(t)$ is the sampled current at time t, C_o, D and S are the concentration (mol cm^{-3}), the diffusion coefficient (cm^2 s^{-1}), and the electroactive area (cm^2), respectively. The diffusion coefficient, $D_{In(III)}$, was calculated from the slope of the straight lines and the results are gathered in Table 1.

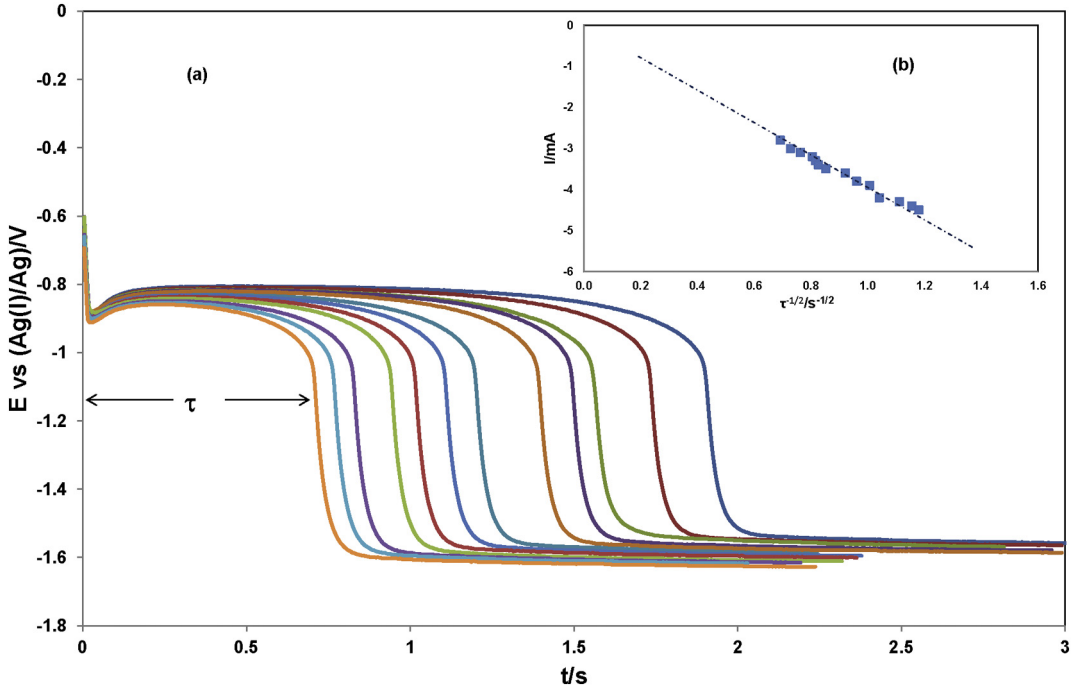

Fig. 12. (a) Evolution of the chronopotentiograms of a $InCl_p^{3-p}$ solution ($C_0 = 6.21 \times 10^{-5}$ mol cm^{-3}) at a tungsten electrode ($S = 0.46$ cm^2) at various applied currents -3.0; -3.1; -3.2; -3.4; -3.5; -3.6; -3.8; -3.9; -4.2; -4.3; -4.4 and -4.5 mA, at 323 K. (b) Relation between square root of transition time and the applied current.

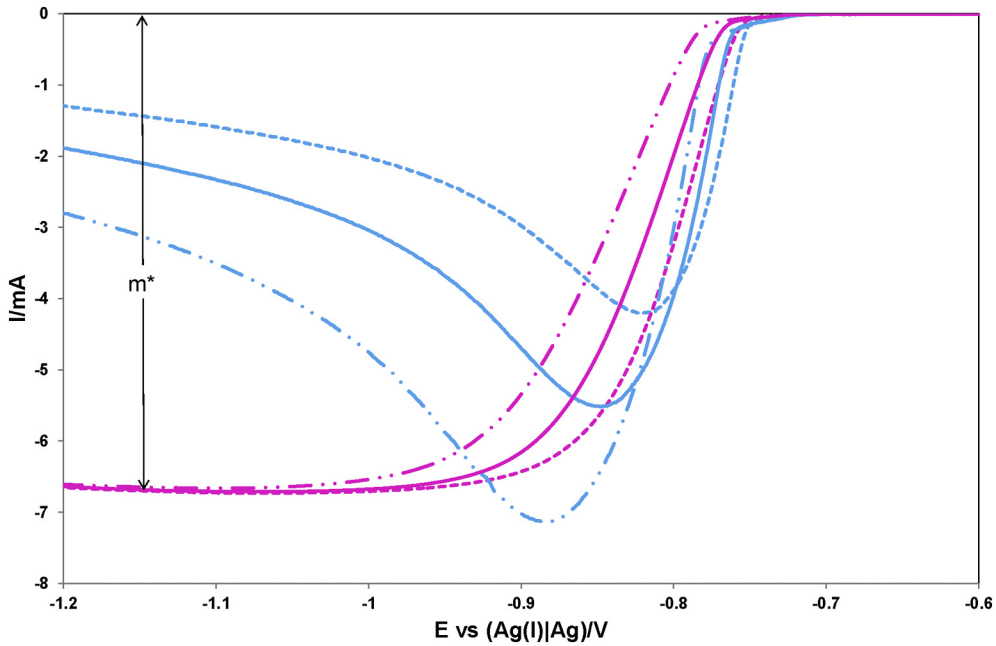

Fig. 13. Evolution of the voltammograms (blue) and convoluted (pink) curves obtained with a $InCl_p^{3-p}$ solution ($C_0 = 6.15 \times 10^{-5}$ mol cm^{-3}) at a tungsten electrode and 343 K, sweep rate: (—) 50, (—) 100 and (–·–) 200 mV s^{-1}. (For interpretation of the references to colour in this figure legend, the reader is referred to the web version of this article.)

3.4.2. Results obtained by chronopotentiometry (CP)

The diffusion coefficient of In(III) was also determined from the chronopotentiograms as those displayed in Fig. 12, by means of Sand's equation [15, 23, 24].

$$I\tau^{1/2} = \frac{nFSD^{1/2}C_0\pi^{1/2}}{2} \quad (15)$$

where I is the applied current and τ is the transition time measured in the chronopotentiograms.

In order to assure the renewal of the electrode and the same electrode/electrolyte interface conditions at the beginning of each chronopotentiogram, the same protocol described in the chronoamperometric experiments was applied.

As it is shown in Fig. 12, the plateau corresponding to the reduction of In(III) can be clearly defined, and as predicted by Sand's equation the transition time becomes shorter increasing the applied current. Likewise, the square root of the transition time changed linearly with the applied current density (Fig. 12 b), indicating that the fluxes of In(III) species were diffusion controlled and that all the requirements for using Sand's equation are fulfilled. The diffusion coefficient was calculated from the slope on Fig. 12b by Eq. (18) being the mean values obtained at different temperatures gathered in Table 1.

3.4.3. Results obtained by convolutive potential sweep voltammetry (CPSV)

The convolution of the cyclic voltammograms recorded at several

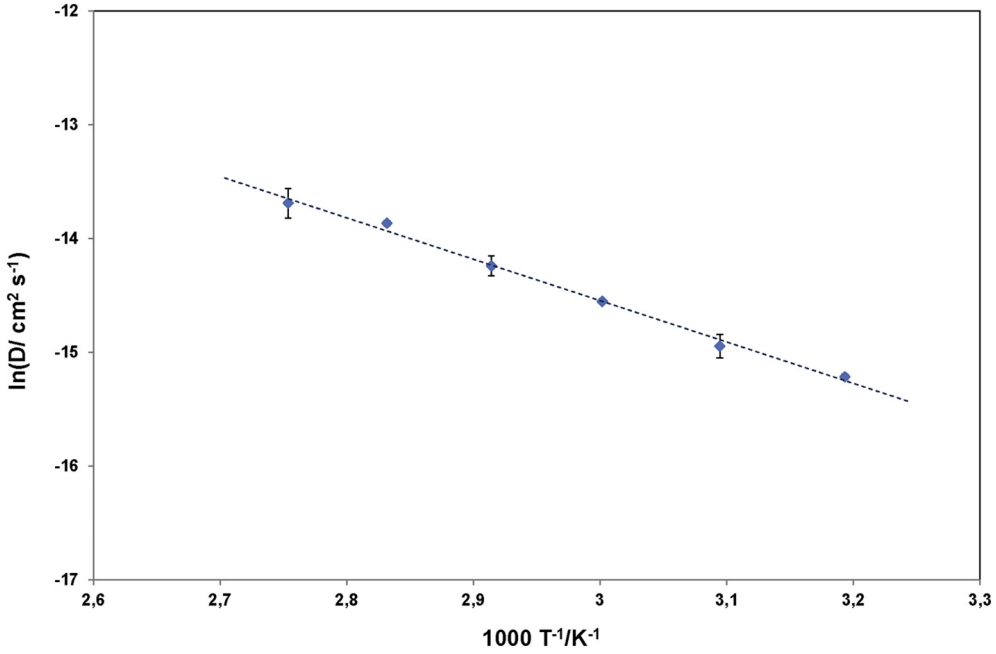

Fig. 14. Variation of diffusion coefficient of In(III) with temperature in ChCl-EG (1:2). Verification of the Arrhenius law.

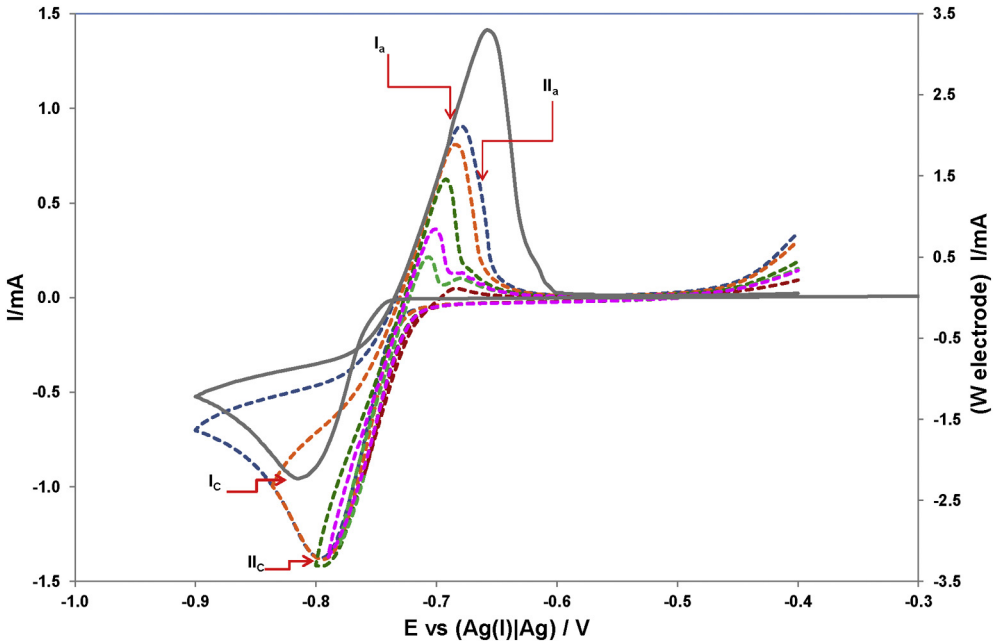

Fig. 15. Cyclic voltammograms obtained at different potential limits (−0.76; −0.78; −0.79; −0,80; −0.85; and − 0.90 V vs Ag(I)/Ag) with a In(III) solution ($C_0 = 7.29 \times 10^{-5}$ mol cm^{-3}) at a W electrode (grey line) and a Cu electrode (dotted lines) at 343 K. Scan rate: 10 mV s^{-1}.

scan rates on a W electrode was also carried out by means of the following expression [15, 23]:

$$m(t) = \frac{1}{\pi^{1/2}} \int_0^t \frac{i(u)}{(t-u)^{1/2}} du \quad (16)$$

where m(t) is the convoluted current, and i(u) the current from the voltammogram.

Fig. 13 depicts examples of the voltammograms recorded with a solution of In(III) and its corresponding semiintegrated curves. In the convoluted curves (pink lines), the peaks have disappeared and instead, a plateau of height m*, is developed at potential values sufficiently cathodic to ensure zero surface concentration of the reactant. The convoluted curves exhibited well defined limiting currents, indicating that there is no change in the electrode surface area during the scan, to the point that it affects the limiting current for the In(III) reduction wave. Hence the In(III) diffusion coefficient could be computed from the boundary semi-integral values by means of the relationship [15,23,24]:

$$m^* = nFSC_0D^{1/2} \quad (17)$$

A summary of the values of the diffusion coefficient obtained by using the aforementioned techniques are displayed in Table 1.

A two-way (temperature - technique) analysis of variance (ANOVA) [25] was carried out in order to know if there are significant differences between the calculated data using: i) different techniques, and ii) different working temperatures, being the null hypothesis the non-

Table 2
Electrolysis experiments and identification of the different phases in the obtained samples.

Potentiostatic electrolysis				
Sample	[In(III)]/mol cm^{-3}	$E_{applied}$ vs (Ag(I)/Ag)/V	Time/s	Identified phase
1	2.6×10^{-5}	−0.8	240	Cu, CuIn
2	6.8×10^{-5}	−0.9	7200	Cu, In, CuIn
3	6.8×10^{-5}	−1.1	3600	Cu, In, CuIn

Intensiostatic pulse electrolysis				
Sample	[In(III)]/mol cm^{-3}	$J_{applied}$/mA cm^{-2}	Time/s	Identified phase
4	2.7×10^{-5}	−0.79 (t_{ON} = 2 s; t_{off} = 4 s)	6340	Cu, In, CuIn
5	6.3×10^{-5}	−2.22 (t_{ON} = 2 s; t_{off} = 6 s)	1040	Cu, In, CuIn
6	6.3×10^{-5}	−2.07 (t_{ON} = 2 s; t_{off} = 6 s)	3230	Cu, In, CuIn

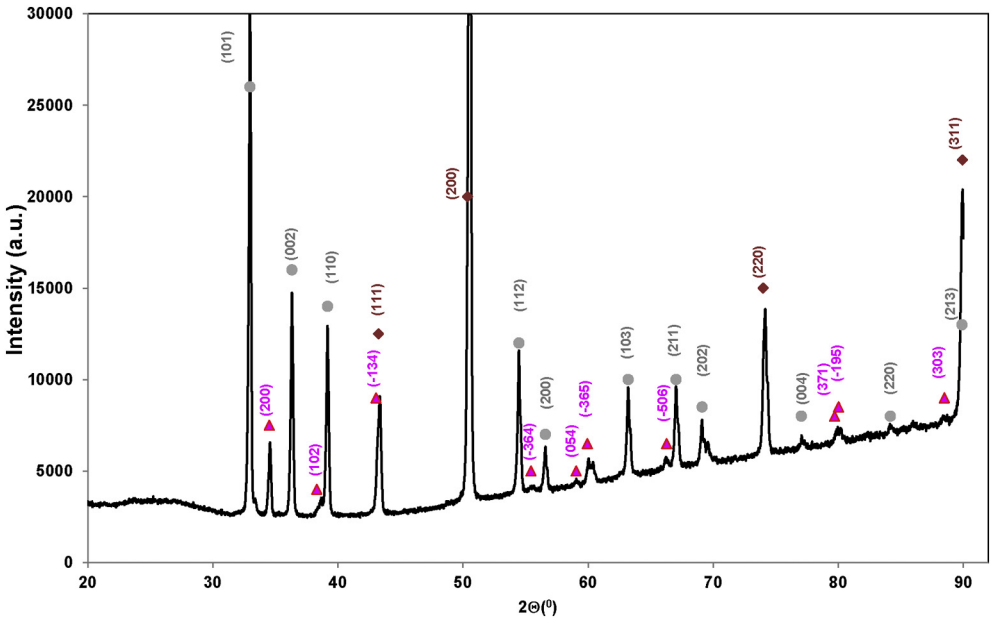

Fig. 16. XRD pattern of sample (3) obtained on a Cu plate from the electrolyte containing $InCl_p^{3-p}$ under potentiostatic electrolysis (Ed = −1.1 V vs Ag(I)/Ag), td = 3600 s). (●) In, (▲) CuIn, (◆) Cu.

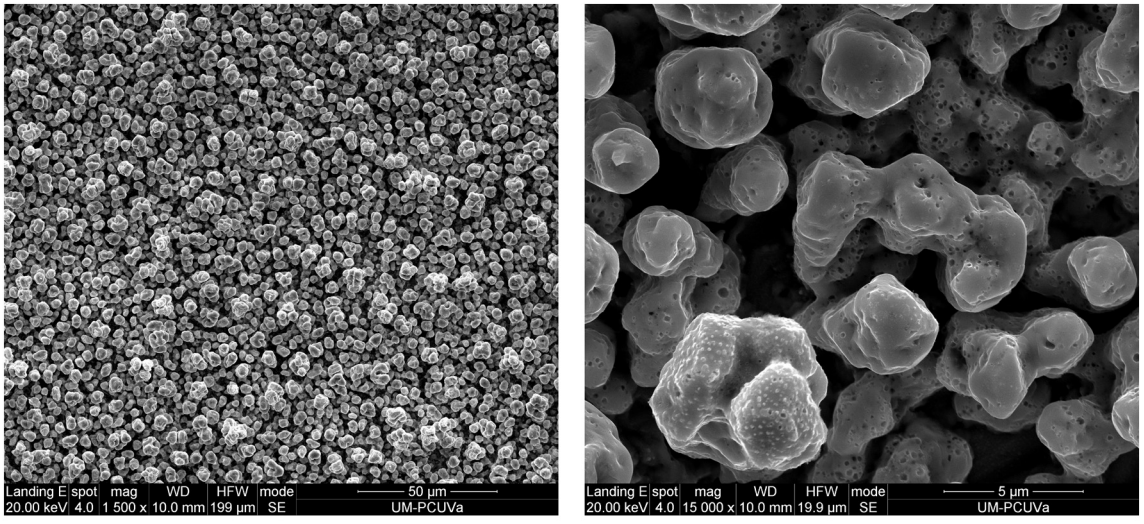

Fig. 17. SEM micrographs of sample (3); (a) surface appearance, (b) details.

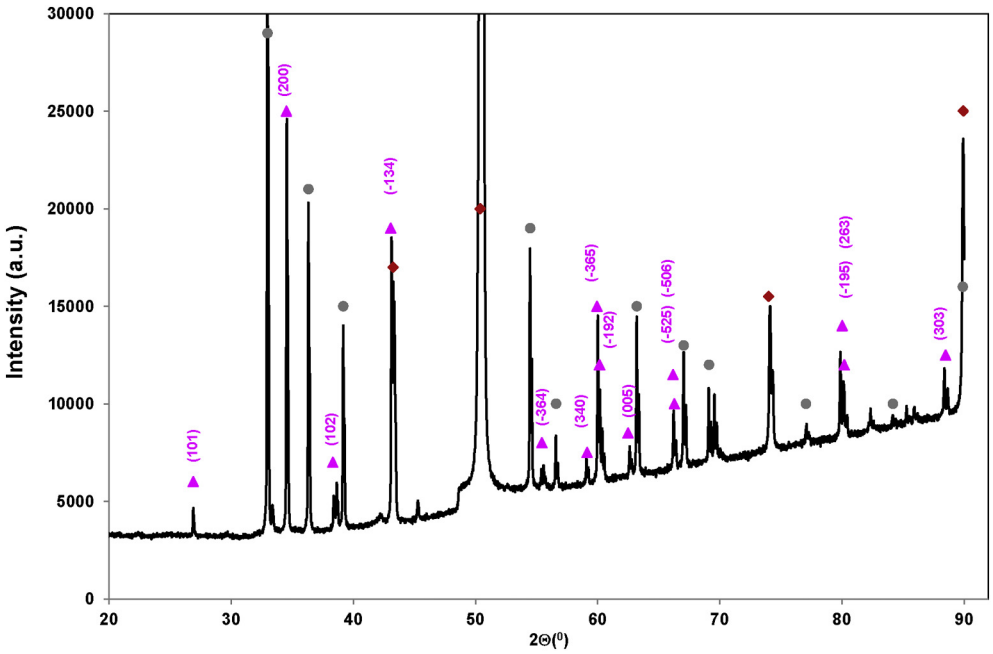

Fig. 18. XRD pattern of sample (6). (●) In, (▲) CuIn, (◆) Cu.

existence of significant differences between the calculated units. Concerning the effect of the techniques, the calculated F statistics was lower than the critical F value ($F_{cal} = 6.02 < F_{crit.} = 6.94$), then the null hypothesis must be maintained. On the contrary, for the temperature effect the calculated F statistics was higher than the critical F value, ($F_{cal} = 103.42 > F_{crit.} = 6.94$) and consequently the null hypothesis must be rejected. As a result, it can be concluded that with a 95% confidence level: i) all the methods used to calculate the diffusion coefficients lead to the same values, and ii) as expected the diffusion coefficients change with temperature. Hence, in order to calculate the activation energy for diffusion, the diffusion coefficient was determined at three more temperatures (313, 333 and 353 K) by using only the convoluted technique due to the simplicity of data acquisition. The obtained diffusion coefficient values showed a good linearity in the Arrhenius plot (Fig. 14), and with a number of observations $n = 103$, it was possible to formulate the following empirical expression for the temperature dependence of the diffusion coefficient of In(III) in ChCl-EG (1:2) as follows:

$$\ln D = -(3.57 \pm 0.21) - (3664 \pm 72) T^{-1} \quad (D_{In}: cm^2\ s^{-1} \text{ and } T: K) \qquad (18)$$

From this relationship, the value of the activation energy, Ea, for the diffusion of In(III), was found to be 30.5 ± 0.6 kJ mol^{-1}.

Additionally, in order to characterize the solute global mass transport through its environment, the effect of the viscosity on the diffusion coefficient has been taken into account through the dimensionless Schmidt number ($Sc = \nu/D$) also reported in Table 1. Experimental kinematic and dynamic viscosities as well as density are also summarized in Table 1.

3.5. Results obtained on solid copper cathodes

To investigate the formation of In-Cu precursors by an electrochemical route, the electrochemical behaviour of In(III) solutions at a copper substrate was also studied by cyclic voltammetry and potentiostatic and intensiostatic electrolysis.

3.5.1. Qualitative information

In Fig. 15 the cyclic voltammograms obtained with an In(III) solution in the eutectic mixture at W and Cu electrodes are compared. As we showed above, when the electrode substrate is an inert electrode an important overpotential must be applied in the cathodic scan, in order to initiate the nucleation and subsequent growth of In. The reaction scheme proceeds according to the following deposition mechanism:

$$InCl_p^{3-p} + 3e^- \rightarrow In(0) + pCl^- \qquad (19)$$

When the scan is reversed, the reduction current continues to flow and the deposition of indium now takes place on a less "hostile" surface of previously deposited In rather than on a bare W electrode, being this fact the cause of the current loop observed in the voltammogram. When the applied potential achieved values higher than the equilibrium potential adopted by the W electrode coated by In, the oxidation peak I_a corresponding to the following dissolution mechanism can be observed:

$$In(0) + pCl^- \rightarrow InCl_p^{3-p} + 3e^- \qquad (20)$$

Conversely, when a Cu electrode was used a peak II_c appears at less cathodic potential values than those for pure In deposition on a W electrode (peak I_c), evidencing that it is not yet necessary to apply the nucleation overpotential required on the W substrate. Due to the possibility of In-Cu alloy formation, the electroreduction of In(III) in peak II_c proceeds according to the following mechanism:

$$InCl_p^{3-p} + 3e^- \rightarrow In(0) + pCl^- \qquad (21)$$

followed by the In reaction with the subjacent substrate Cu.

$$In(0) + x\,Cu(0) \rightarrow Cu_xIn \qquad (22)$$

being the overall process:

$$InCl_p^{3-p} + x\,Cu(0) + 3e^- \rightarrow Cu_xIn + pCl^- \qquad (23)$$

When the scan is reversed, in the anodic region two oxidation peaks are displayed, the peak I_a due to the oxidation of In(0) and the peak II_a due to the oxidation of Cu_xIn.

$$\text{Peak } I_a \qquad In(0) + pCl^- \rightarrow InCl_p^{3-p} + 3e^- \qquad (24)$$

$$\text{Peak } II_a \qquad Cu_xIn + pCl^- \rightarrow InCl_p^{3-p} + x\,Cu(0) + 3e^- \qquad (25)$$

3.5.2. Potentiostatic and intensiostatic electrolysis. Characterization of the In-Cu alloys

Based on the previous results, alloys samples were prepared by both potentiostatic and intensiostatic electrolysis. All the experiments were conducted using 0.5 mm copper plates as working electrodes. After electrolysis, the samples were washed by immersion in ultrapure water

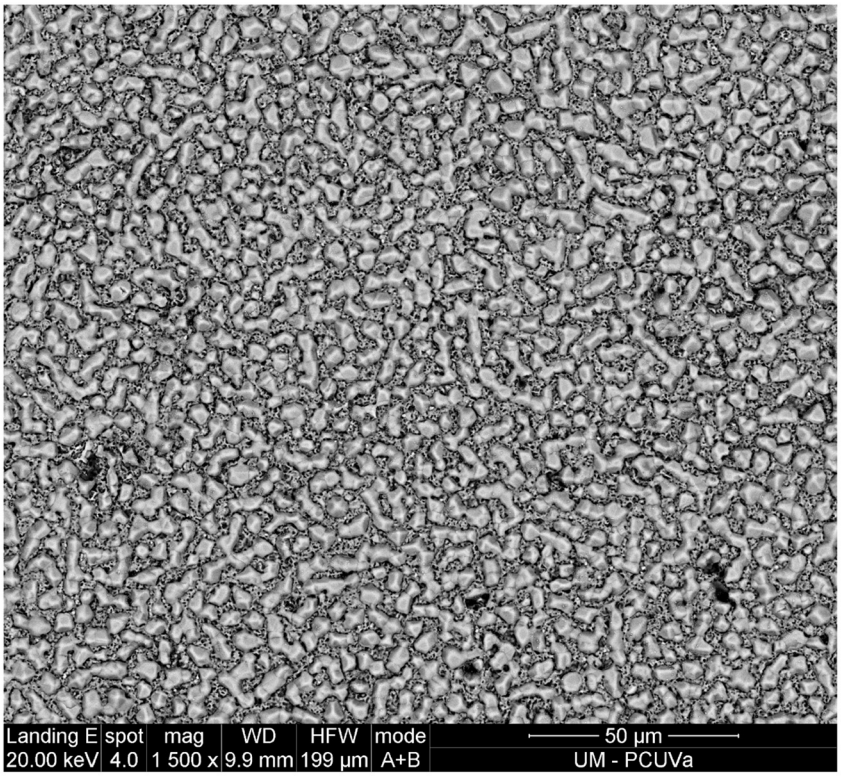

A

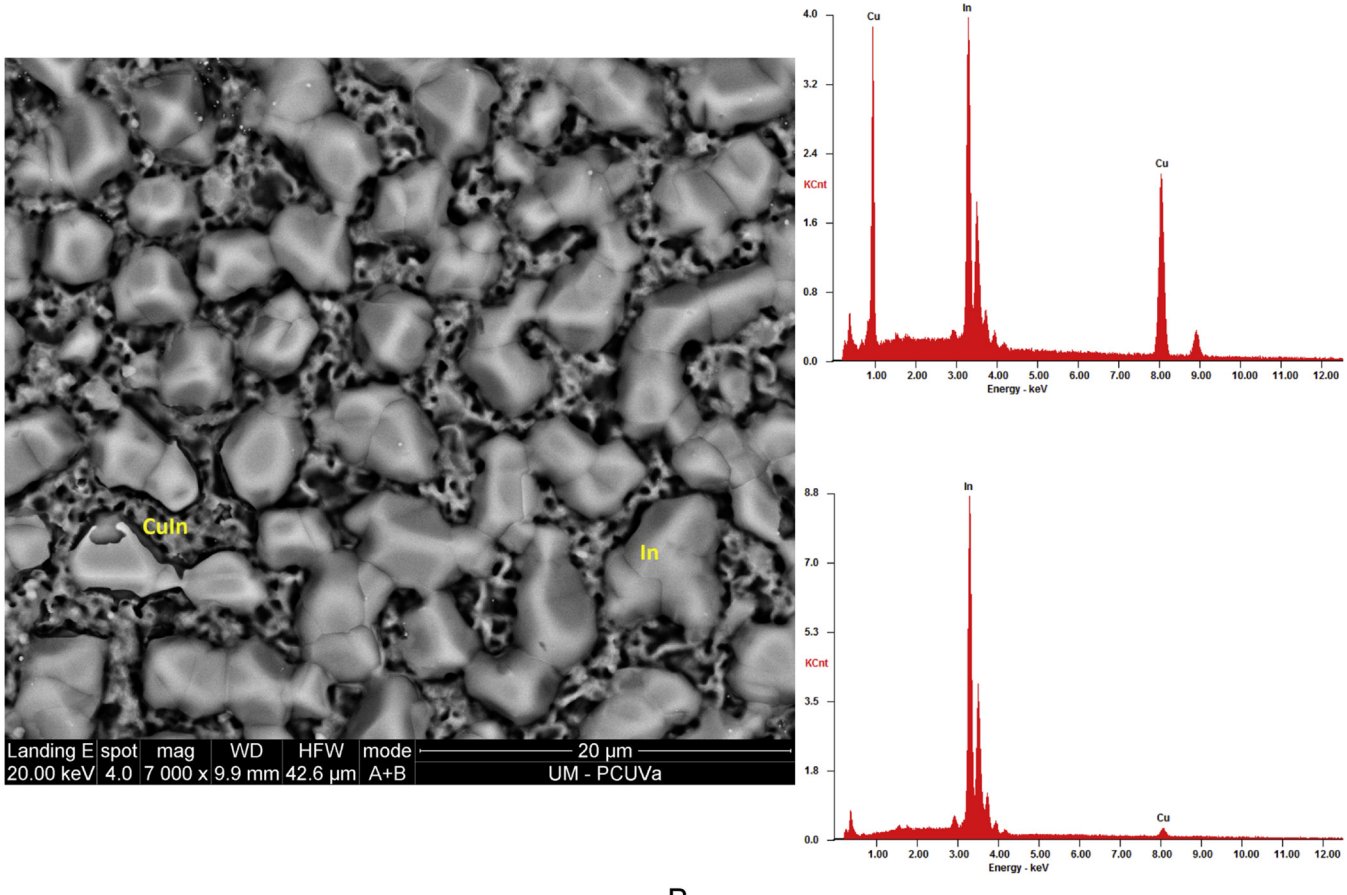

B

Fig. 19. SEM micrographs of sample (5); (a) surface appearance, (b) details and EDXs.

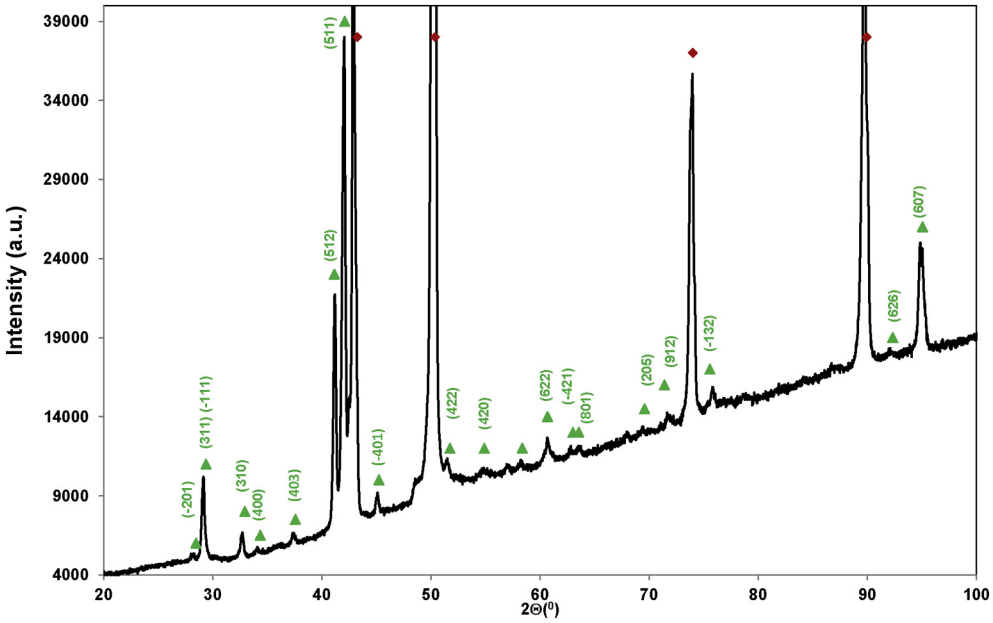

Fig. 20. XRD pattern of sample (5) after annealing at 430 K for 2 h. (▲) $Cu_{11}In_9$, (◆) Cu.

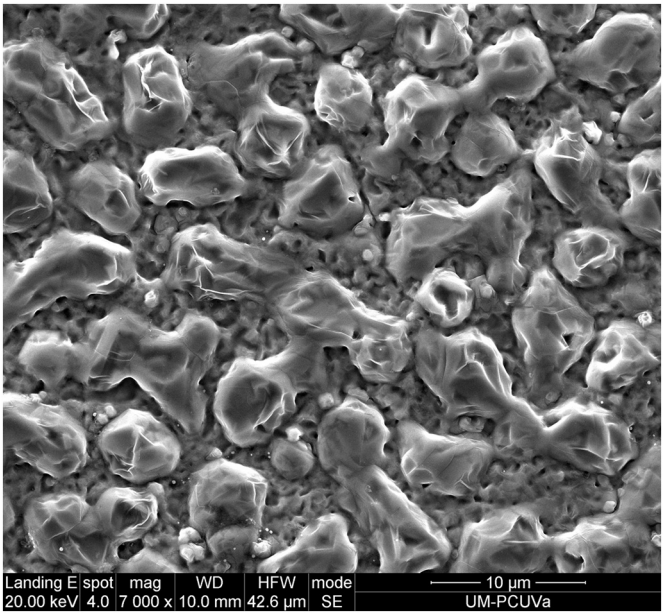

Fig. 21. SEM micrograph of sample (5) after annealing.

Milli-Q, and finally in ethanol. The dried samples were analysed by XRD, SEM and EDAX techniques. A summary of the XRD analysis is gathered in Table 2.

Samples (1–3) obtained under potentiostatic conditions provided similar results. Fig. 16 shows the XRD pattern of sample (3) obtained at −1.1 V vs (Ag(I)/Ag). The observed peaks were identified as CuIn, In and Cu substrate, being the intensities of the Cu and In peaks predominant over those of the CuIn phase, which shows that the thickness of the CuIn film on the Cu substrate was thin. The surface morphology of the obtained deposit was also observed by scanning electron microscopy (SEM) (Fig. 17 (a–b)).The deposit is made up of clusters vertically aligned and parallel to each other, making the surface of the deposit porous.

Intensiostatic pulse electrolysis was also conducted. Each pulse consists of an ON-Time (t_{ON}) during which a current is applied, and an OFF-Time (t_{OFF}) during which no current is applied, in order to allow In diffusion into the massive Cu plate. The XRD analysis of samples (4–6) also evidence the formation of the stoichiometric phase CuIn (Fig. 18).

The surface morphology of sample (5) was also observed by SEM and analysed by EDAX. Fig. 19 (a–b) show compact clusters of In over a network-like structure of the intermetallic CuIn. The effect of annealing on the crystal structure of thin film of sample (5) is shown in Fig. 20, observing that the metastable phase CuIn obtained at 343 K can be transformed into $Cu_{11}In_9$ at a higher temperature (e.g. 430 K). The surface morphology is also displayed in Fig. 21.

4. Conclusions

A procedure for drying the DES, ChCl-EG (1:2), based on the use of molecular sieves has been developed, being the water content of the electrolyte 145 ± 5 ppm.

The stability of anhydrous InCl and $InCl_3$ dissolved in the dried DES has been investigated using cyclic voltammetry, x-Ray diffraction analysis and scanning electron microscopy. Experiments performed in a controlled N_2 atmosphere cell, show that anhydrous $InCl_3$ dissolved in the rich chloride media as $InCl_p^{3-p}$ is reduced on an inert electrode (i.e W) to indium metal via only one electrochemical step. Conversely, InCl undergoes the following disproportionation reaction when dissolved in the eutectic ChCl-EG (1:2).

$$3InCl(s) + (p - 3)Cl^- \rightleftharpoons 2In(0) + InCl_p^{3-p}$$

generating In(0) and $InCl_p^{3-p}$ that provides identical voltammograms as those obtained after the addition of $InCl_3$ to the DES.

The electrochemical behaviour of $InCl_p^{3-p}$ solutions has been studied using different substrates: i) W, an inert working electrode, and ii) Cu, a more noble metal than In with possibility of alloy formation.

Voltammetric and chronoamperometric experiments on a W electrode showed that nucleation and growth of the metallic indium plays an important role in the overall electrodeposition process. Chronoamperometric studies showed that the deposition process on the inert electrode involves, whatever the applied overpotential, instantaneous three dimensional nucleation on a finite number of active sites with diffusion controlled growth of the nuclei. Not being the nucleation mode of indium influenced by temperature in the 323–363 K range.

The applicability of several electrochemical techniques (CA, CP and CPSV) for accuracy measurements of the diffusion coefficient of $InCl_p^{3-p}$ was also investigated, verifying the validity of the assumptions used in their theoretical analysis, and ensuring reproducible conditions at the

electrode/electrolyte interface. A two-way analysis of variance, ANOVA has shown that with a 95% confidence level: i) the three electrochemical techniques used to calculate the diffusion coefficients lead to the same values, and ii) the diffusion coefficient changes with temperature following the Arrhenius law, being the activation energy for diffusion 30.5 ± 0.6 kJ mol^{-1}. The dimensionless Schmidt numbers, defined as the ratio between solvent viscosity and solute diffusivity ($Sc = \nu/D$), have also been calculated to characterize the solute global mass transport through its environment.

To investigate the formation of In-Cu precursors by an electrochemical route, the electrochemical behaviour of In(III) solutions at a copper substrate was also studied by cyclic voltammetry and potentiostatic and intensiostatic electrolysis. The resulting cyclic voltammograms exhibited signals that could be attributed to the presence of In-Cu intermetallic compounds. Thin layers of the intermetallic compounds were obtained by electrosynthesis and characterized by X-ray diffraction and scanning electron microscopy (SEM) revealing in all cases the formation of stoichiometric CuIn. The metastable CuIn phase was transformed into $Cu_{11}In_9$ by thermal annealing.

The deposits obtained under continuous potentiostatic electrolysis were made up of clusters vertically aligned and parallel to each other, making the surface of the deposits porous. Conversely, the films obtained by intensiostatic pulse electrolysis consisted on compact clusters of In over a network-like structure of the stoichiometric CuIn.

Acknowledgements

Authors thank the Consejería de Educación of the Junta de Castilla y León Project VA171U14 for financial support. S. García, also thanks the youth employment operative programme (European Social Fund, ESF, and youth employment initiative, YEI).

References

[1] A.A.C. Alcanfor, L.P.M. dos Santos, D.F. Dias, A.N. Correia, P. de Lima-Neto, Electrodeposition of indium on copper from deep eutectic solvents based on choline chloride and ethylene glycol, Electrochim. Acta 235 (2017) 553–560.
[2] D.D. Shivagan, P.J. Dale, A.P. Samantilleke, L.M. Peter, Electrodeposition of chalcopyrite films from ionic liquid electrolytes, Thin Solid Films 515 (2007) 5899–5903.
[3] N.B. Chaure, J. Young, A.P. Samantilleke, I.M. Dharmadasa, Electrodeposition of p–i–n type $CuInSe_2$ multilayers for photovoltaic applications, Sol. Energy Mater. Sol. Cells 81 (2004) 125–133.
[4] S. Sanchez, C. Lucas, G.S. Picard, M.R. Bermejo, Y. Castrillejo, Molten salt route for ZnSe high-temperature electrosyhthesis, Thin Solid Films 361-362 (2000) 107–112.
[5] M. Steichen, M. Thomassey, S. Siebentritt, P.J. Dale, Controlled electrodeposition of Cu-Ga from a deep eutectic solvent for low cost fabrication of $CuGaSe_2$ thin film solar cells, Phys. Chem. Chem. Phys. 13 (2011) 4292–4302.
[6] E.L. Smith, A.P. Abbott, K.S. Ryder, Deep Eutectic Solvents (DESs) and their applications, Chem. Rev. 114 (2014) 11060–11082.
[7] L. Vieira, A.H. Whitehead, B. Gollas, Mechanistic studies of zinc electrodeposition from deep eutectic electrolytes, J. Electrochem. Soc. 161 (1) (2014) D7–D13.
[8] S. Ghost, S. Roy, Electrochemical copper deposition from an ethaline –$CuCl_2{\cdot}2H_2O$ DES, Surf. Coat. Technol. 238 (2014) 165–173.
[9] J.C. Malaquias, M. Steichen, M. Thomassey, P.J. Dale, Electrodeposition of Cu-In alloys from a choline chloride based deep eutectic solvent for photovoltaic applications, Electrochim. Acta 103 (2013) 15–22.
[10] K. Haerens, E. Matthijs, K. Binnemns, B. Van der Bruggen, Electrochemical decomposition of choline chloride based ionic liquid analogues, Green Chem. 11 (2009) 1357–1365.
[11] F. Feigl, V. Anger, Spot Tests in Inorganic Analysis, Elsevier, Amsterdam, The Netherlands, 1972.
[12] A.H. Whitehead, M. Pölzler, B. Gollas, Zinc electrodeposition from a deep eutectic system containing choline chloride and ethylene glycol, J. Electrochem. Soc. 157 (6) (2010) D328–D334.
[13] L. Vieira, R. Schennach, B. Gollas, The effect of the electrode material on the electrodeposition of zinc from deep eutectic solvents, Electrochim. Acta 197 (2016) 344–352.
[14] J.S. Liu, I.W. Sun, Electrochemical study of properties of indium in room temperature chloroaluminate molten salts, J. Electrochem. Soc. 144 (1997) 140–145.
[15] Southampton Electrochemistry Group, Instrumental Methods in Analytical Chemistry, University of Southampton, Horwood, Chichester, 2001.
[16] B. Scharifker, G. Hills, Theoretical and experimental studies of multiple nucleation, Electrochim. Acta 28 (1983) 879–889.
[17] B. Scharifker, J. Mostany, Three-dimensional nucleation with diffusion controlled growth. Part I. Number density of active sites and nucleation rates per site, J. Electroanal. Chem. 177 (1984) 13–23.
[18] P.M. Rigano, C. Mayer, T. Chierchie, Electrochemical nucleation and growth of copper on polycrystalline palladium, J. Electroanal. Chem. 248 (1988) 219–228.
[19] W.R. Pitner, C. Hussey, G.R. Stafford, Electrodeposition of nickel-aluminium alloys from the aluminum chloride-1-methyl-3-ethylimidazolium chloride room temperature molten salt, J. Electrochem. Soc. 143 (1996) 130–138.
[20] X. Xu, C.L. Hussey, The electrochemistry of tin in the aluminum chloride-1-methyl-3-ethylimidazolium chloride molten salt, J. Electrochem. Soc. 140 (1993) 618–626.
[21] M. Palomar-Pardavé, I. González, A.B. Soto, E.M. Arce, Influence of the coordination sphere on the mechanism of cobalt nucleation onto glassy carbon, J. Electroanal. Chem. 443 (1998) 125–136.
[22] E. Barrado, J.A. Rodríguez, Y. Castrillejo, A comparative study of the cathodic behaviour of $EuCl_3$ in two imidazolium chloride ionic liquids, the 1-butyl-3-methylimidazolium (C_4mimCl) and the 1-ethyl-3-methylimidazolium (C_2mimCl), on a glassy carbon electrode, J. Electroanal. Chem. 804 (2017) 148–157.
[23] A.J. Bard, L.R. Faulkner, Electrochemical Methods: Fundamentals and Applications, Wiley, New York, 2001.
[24] K.B. Oldham, J.C. Myland, A.M. Bond, Electrochemical Science and Technology: Fundamentals and Applications, Wiley & Sons, Ltd, 2013.
[25] D.M. Massart, B.G.M. Vandeginste, L.M.C. Buydens, S. de Jong, P.J. Lewi, J. Smeyers-Verbeke, Handbook of Chemometrics and Qualimetrics, Elsevier, Amsterdam, 1997.